CSEM data uncertainty analysis for 3D inversion

Jan Petter Morten*, EMGS, Astrid Kornberg Bjørke, EMGS, and Trude Støren, EMGS

SUMMARY

Inaccurate navigation can be an important source of measurement errors in CSEM data. Improved algorithms for estimating receiver orientation yield values for the uncertainty in the resulting angles. We show how linear error propagation analysis can be used for improved 3D inversion by accounting for such uncertainty in the data weighting scheme.

INTRODUCTION

In an inverse problem, model parameters are estimated from measured data (Tarantola, 2005). All measurements are associated with uncertainties due to limitations of the experiment and instrument precision. Therefore, it is important to take uncertainty into account in the inversion algorithm to avoid model reconstruction on the basis of inaccurate or erroneous data. Classical formulations of the inverse problem deal with this problem using data sample weights that represent the measurement uncertainty, and regularization which introduces assumptions on the features of the inversion model.

Subsurface resistivity imaging based on marine controlled source electromagnetic (CSEM) data (Constable and Srnka, 2007) is a special case of the inverse problem. Effective tools for such processing have been developed and successfully applied in the context of hydrocarbon exploration and volume estimation (Jing *et al.*, 2008; Støren *et al.*, 2008). A recent development in data acquisition is the use of 3D receiver grids, where azimuth data recorded by receivers off the source towlines provides additional information regarding anisotropy and the background resistivity distribution, as well as extended data coverage compared to inversion of in-line data only. The azimuth data is especially important for 3D inversion of CSEM data from coarse receiver grids used in exploration type, scanning surveys (Morten *et al.*, 2009).

As the amount of collected data and the precision and predictive power of advanced data processing tools such as 3D inversion develops, the demands on the data accuracy also increase. Inaccurate data and noise will be reflected in the reconstructed models unless handled properly, and can lead to confusing results if artifacts cannot easily be separated from geologically realistic features. The sources of measurement error can be random or systematic.

An important parameter in a CSEM measurement is the orientation of the seafloor receivers. The orientation is used to determine the electromagnetic field vectors, and can be measured to high precision by equipping the receivers with gyroscopes. However, such instruments are very costly and usually the orientation must be estimated from the data itself. The estimation methods have fundamental accuracy limitations, which can make them an important source of systematic error. In

contrast, we expect minor contributions to measurement uncertainty from source navigation and receiver position in CSEM data, which are measured to high accuracy using acoustic triangulation.

Improved methods for orientation estimation that can integrate far-offset and azimuth data have been developed, and the results compare well to gyroscope measurements on real data. One of the methods involves plane-layer inversion of single receiver data, where the receiver orientation is one of the free parameters in the optimization (Mittet *et al.*, 2004). Important complementary information provided by this method is estimates of the uncertainty in receiver orientation. This data can be very valuable as the sensitivity to inaccurate orientation varies considerably with the source-receiver configuration. We will in the following show how this information can be integrated in the 3D inversion algorithm.

Calibration of the electric and magnetic field sensors can be an additional source of systematic error which needs to be taken into account. Finally, the measurements are always affected by random instrument noise and environment noise due to e.g. magnetotelluric (MT) activity (de la Kethulle de Ryhove and Maaø, 2008).

In this abstract, we show the importance of taking the sensitivity to orientation inaccuracies in CSEM data into account when inverting azimuth data from 3D grids. Linear error propagation is utilized to find the configuration dependent uncertainty of data samples, and these results are used to compute the inversion data weights. Using the rotation uncertainty provided by the orientation estimation method, such analysis can give significantly improved 3D inversion results.

ERROR PROPAGATION ANALYSIS

A standard CSEM data processing step is to estimate the orientation of the magnetic and electric field sensors, and "rotate" the data so that it represents the measurements had the receiver been oriented with one axis parallel to an "overflight" source towline. The resulting in-line rotated field components are given by

$$\begin{pmatrix} F_x \\ F_y \end{pmatrix} = \begin{pmatrix} \cos\phi & \sin\phi \\ -\sin\phi & \cos\phi \end{pmatrix} \begin{pmatrix} F_a \\ F_b \end{pmatrix}, \qquad (1)$$

where F_i represents a horizontal component ($i = x, y$ for rotated data, or a, b for the data before rotation) of the electric ($\mathbf{F} = \mathbf{E}$) or magnetic ($\mathbf{F} = \mathbf{H}$) field, and ϕ is the estimated angle between the direction of the seafloor receiver measurement channel F_a and the source towline direction.

The E_x and H_y components of in-line rotated data are usually not very sensitive to small orientation errors introduced by inaccurate estimation of ϕ. Typically, a small orientation estimation error when rotating the data to inline-configuration gives

a small variation in this data. The reason can be seen from standard error propagation analysis, which estimates the error of the derived quantities F_x and F_y from errors in the measurements. In this analysis, we take into account a constant relative error in the field amplitude measurements $\alpha = |\Delta F_i/F_i|$ $(i = a, b)$, which is typically a few percent and mainly caused by instrument calibration inaccuracy. The absolute error in the angle used to rotate the receiver in-line is denoted $\Delta\phi$ and is associated with limitations of the orientation estimation. In these notations, the magnitude errors of in-line rotated data become

$$|\Delta F_x| = \sqrt{\alpha^2 \left(|F_a|^2 \cos^2\phi + |F_b|^2 \sin^2\phi\right) + |F_y|^2 (\Delta\phi)^2},$$

(2a)

$$|\Delta F_y| = \sqrt{\alpha^2 \left(|F_a|^2 \sin^2\phi + |F_b|^2 \cos^2\phi\right) + |F_x|^2 (\Delta\phi)^2}.$$

(2b)

Let us consider E_x data from a receiver on the source towline and use the result Eq. (2a). Note that the term inside the square root depending on $\Delta\phi$ is proportional to E_y. Due to the horizontal dipole field distribution (see Figure 1), this component usually has a much smaller magnitude than E_x so the contribution to the total error associated with $\Delta\phi$ will be small. This is a desired property of the experiment, since the most valuable information about possible thin resistors in in-line data will be described by E_x which has the maximum energy. Conversely, the sensitivity to errors in ϕ is large for E_y in-line data according to Eq. (2b).
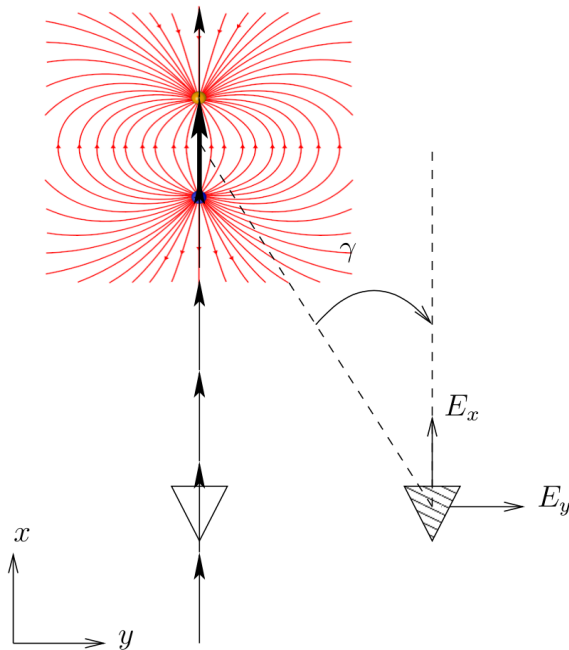

Figure 1: Schematic horizontal electric dipole source and receiver configurations. Open triangle denotes in-line receiver, and shaded triangle denotes "azimuth receiver" located off the source towline. Source positions are indicated by arrows, and dipole field lines (red) are indicated for the emphasized (thick arrow) source position.

For azimuth data, the offset dependence of measurement un-

certainty is more complicated. In data collected by receivers off the source towline, the relative magnitudes of the two horizontal field components varies with the angle between the source-receiver vector and the towline direction, denoted γ, see Figure 1. Close to the broadside ($\gamma = 90°$) configuration, the E_y field component can have larger magnitude than the E_x component, and the E_x data is the more uncertain. For some offsets, the E_x field component associated with the source dipole can even go through a sign change, and the data in this offset interval is very sensitive to orientation error. At long offsets, the source-receiver configuration becomes more similar to that of an in-line receiver with γ small so that $|E_y| \ll |E_x|$. Thus Eqs. (2) show that for azimuth data, both horizontal data channels can be very sensitive to orientation estimation errors $\Delta\phi$.

3D INVERSION DATA WEIGHTS

The inversion process results in a model which by 3D modeling reproduces the survey data to within the measurement accuracy. The model is obtained by minimizing the square weighted L^2 norm of the complex difference between observed ($\mathbf{F}^{\text{Obs}}$) and synthetic (modeled) ($\mathbf{F}^{\text{Synth}}$) data,

$$\sum_{F,\kappa} W_{F,\kappa}^2 \left| F_\kappa^{\text{Obs}} - F_\kappa^{\text{Synth}} \right|^2.$$

(3)

Here, the index κ denotes all running variables of the dataset to invert including offset, frequency, field component etc. The data weight factor $W_{F,\kappa}$ represents the uncertainty of the data sample, and also normalizes the magnitudes of the terms in the sum.

When some parts of the observed data have high sensitivity to inaccuracies in the measured quantities, these data samples can be considered uncertain and should be assigned a low weight in Eq. (3). We use the information about error propagation described by Eqs. (2) to compute the weights,

$$1/W_{F,\kappa}^2 = \left| \Delta F_\kappa^{\text{Obs}} \right|^2 + \eta^2 \left| F_\kappa^{\text{Noise}} \right|^2.$$

(4)

Here η is a constant factor and F_κ^{Noise} is the noise floor representing the background signal level. The noise is estimated in a data processing step by averaging over frequency windows close to the source signal frequency (Zach *et al.*, 2008). The noise floor estimate is additionally used to define a signal-to-noise threshold for data to be included in the inversion. Finally, the weights incorporate masks tagging bad data samples that are omitted, *i.e.* have weight zero. These masks are created in a spike detection processing step.

Systematic tests on synthetic data where we artificially introduced erroneous orientation clearly demonstrates the value of taking orientation uncertainty into account in inversion. Figure 2 shows unconstrained inversion results from a dataset consisting of three survey lines including azimuth data over a rectangular resistor in a homogeneous formation. The data from each receiver was perturbed by rotating by a random angle drawn from a gaussian distribution with standard deviation $10°$. In one case, the orientation error was not taken into account in the

weights ($\Delta\phi = 0$), and in the other case we used $\Delta\phi = 10°$ in the weights computed using Eq. (4). As we can see, the rectangular shaped resistor of the true model is consistently imaged at the correct depth interval only when we take the orientation error into account. Moreover, the the result for $\Delta\phi = 0$ (upper panel) has considerable artifacts in the shallow subsurface.
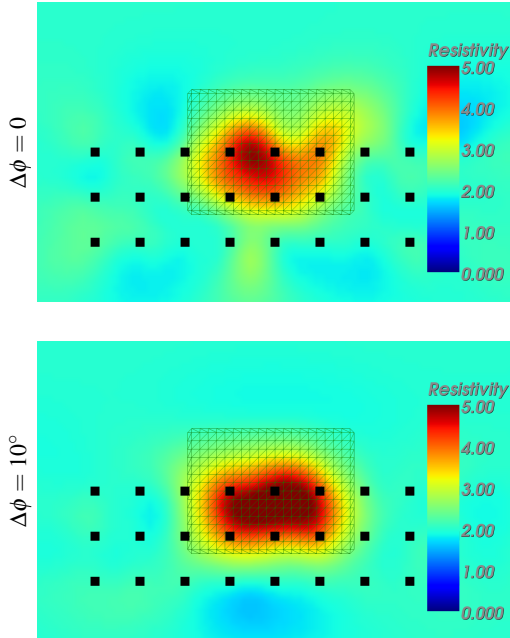

Figure 2: Synthetic data inversion results where random orientation errors were introduced in the data. Upper panel: $\Delta\phi = 0$ *i.e.* orientation uncertainty not taken into account, lower panel: $\Delta\phi = 10°$. The true model contains a 4 km×4 km×50 m resistor at 25 Ωm buried 1 km below the seafloor in a homogeneous formation (true position indicated by shading). The water depth was 1 km and data at 0.25 Hz was inverted. Receiver positions indicated by squares. Data from all three receiver lines for each source towing was included.

TROLL OIL FIELD REAL DATA EXAMPLE

We have tested the approach described above using data from an extensive 3D survey acquired in 2008 over the North Sea Troll oil and gas field. This survey was carried out within an R&D collaboration between EMGS and StatoilHydro, and addressed several topics for the development of next generation CSEM acquisition and interpretation. Here we focus on the 3D dense receiver grid data aimed at detecting thin oil zones in the oil province (Figure 4).

Figure 3 shows the horizontal electric field data from an in-line receiver close to the oil field, as well as azimuth data from the same receiver when the source towline was offset 1.5 km. In addition to the field recordings, the plots show error bars given by the inverse weights $1/W_{F,\kappa}$ following from Eq. (4). The parameters for the measurement uncertainty are as follows: The value $\alpha = 1\%$ is representative for the relative uncertainty of
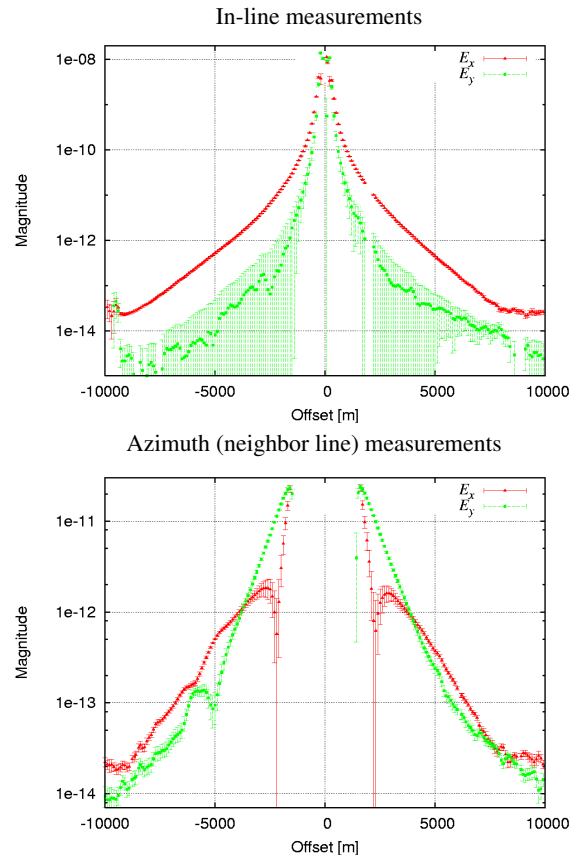

Figure 3: In-line (upper panel) and azimuth (lower panel) data (note different scale) from a receiever in the 2008 Troll oil and gas field 3D survey. The data is rotated so that the E_x axis of the receiver corresponds to the source towline direction. The measurements from the E_x and E_y channels at 0.25 Hz are shown. The error bars are the inverse weights $1/W_{\kappa,F}$ following from Eq. (4).

the field magnitude sensors due to limitations in the instruments and calibration. A rotation uncertainty $\Delta\phi = 3.6°$ was estimated for this receiver in the process of determining the receiver orientation. This value varies with the environment noise and complexity of the local geology at the receiver position. Values in the interval $2 - 4°$ are typical for the Troll 2008 survey. The noise level described by F_κ^{Noise} is computed from the background signal level at the source frequency, and the prefactor $\eta = 1.0$.

The in-line E_x data shown in the upper plot of Figure 3 is very consistent even at far offset ~ 10 km, whereas the in-line E_y data is more strongly affected by noise due to the low magnitude. These features are reflected also by the error bars in the plots. The field magnitudes decay exponentially with the offset, and for the entire offset range $|E_y| \ll |E_x|$.

The azimuth data shown in the lower panel of Figure 3 has a more complicated offset dependence. The data at the shortest offset in the figure corresponds to one source towline spacing (neighbor line receiver), where the receiver is broadside with

$\gamma \approx 90°$. At offsets ~ 2.1 km, corresponding approximately to $\gamma \approx 45°$, we see that $|E_x| \ll |E_y|$ and the associated error bars are large. This offset interval of the E_x azimuth data is especially sensitive to errors in the orientation estimation since a small error in ϕ can give a large error in the data. Therefore, it is important to give little weight to these samples in the inversion input, *i.e.* Eq. (3). If these data are weighted on the same scale as more reliable data, artifacts will be introduced in the reconstruction unless prohibited by strong regularization. At longer offsets $\gtrsim 5$ km, the E_x component can again start to dominate and has the smaller uncertainty. At far offsets, the behavior is similar to in-line data with $|E_y| \ll |E_x|$.
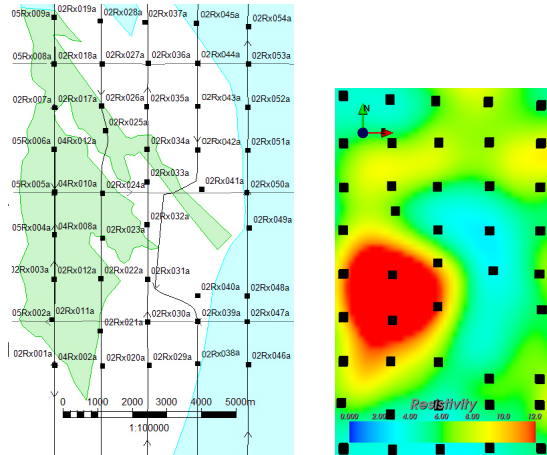

Figure 4: Left panel: Survey layout where towlines are indicated by black lines and receiver positions by squares. The green area in the left/West is the prospect outline for the oil province, and the blue area in the right/East is the gas province prospect outline. Data coverage is non-uniform in the lower right part of the receiver grid due to a deviated source towline to avoid installations in the area. Right panel: Horizontal section at 1480 m from inversion of the 2008 Troll 3D survey using the horizontal electric fields and data at frequencies 0.25, 0.75, and 1.25 Hz. Black dots indicate receiver positions.

In the following, we consider unconstrained inversion of a selection of the Troll 2008 dataset, which includes azimuthal data from neighbor receiver lines separated up to 6 km from the source towlines. We include data from source towings along five North-South directed towlines, as well as three orthogonal East-West directed towlines. Altogether, the dataset includes magnitude and phase recordings from 44 receivers. The survey layout and a horizontal slice through the 3D inversion result is shown in Figure 4. The lateral extension of the oil province reconstructed resistor corresponds well to information from seismic and well logs. Thin (40 m) oil zones at the edges of the prospect are imaged, as well as gas accumulations in the center. Parts of the Troll gas province, which is outside the receiver grid, is also reconstructed. Figure 5 shows a vertical cross section of the 3D inversion result along the center of the oil field prospect. The figure also shows a 3D prospect outline based on seismic. The reconstructed resistor is placed at the correct depth, and the typical resistivity inside the anomaly is 15 Ωm. There are no prominent artifacts in this

image, indicating that the uncertainty-sensitive measurements in the dataset are suppressed appropriately. Anisotropic 3D inversion was also carried out, and the reconstructed resistors are similar.
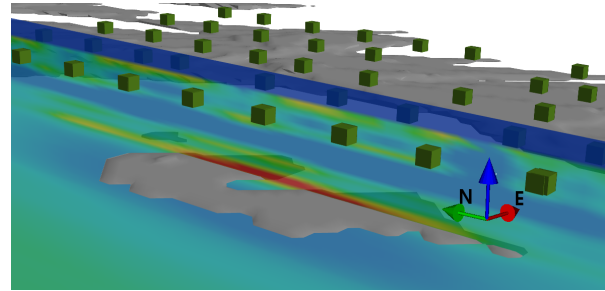

Figure 5: Vertical section along the center of the Troll oil province reconstruction (*i.e.* between the two survey lines farthest West in Figure 4, as well as 3D seismic anomaly outline (grey volume) and receiver positions (green boxes). The resistor is placed at depth 1480 m below sea level, which corresponds with top reservoir horizon. The thickness of the resistor is 110 m in the middle part. The colorscale is the same as in Figure 4.

CONCLUSION

We have described how the sensitivity to error in the receiver orientation estimation of 3D CSEM data varies with the offset and source-receiver configuration. Particularly, we focus on the azimuth data which are essential for inversion of coarse receiver grid scanning data, and which carry important information about anisotropy. Processing workflows that result in estimates of the uncertainty of the receiver orientation angle as well as the angle itself can be utilized to compute 3D inversion data weights that reflect the confidence of each data sample. Real data examples demonstrate how the weight corresponds to the uncertainty of the measurement. Resulting inverted models have only small artifacts and clearly images known thin oil zones.

ACKNOWLEDGMENTS

EDITED REFERENCES

Note: This reference list is a copy-edited version of the reference list submitted by the author. Reference lists for the 2009 SEG Technical Program Expanded Abstracts have been copy edited so that references provided with the online metadata for each paper will achieve a high degree of linking to cited sources that appear on the Web.

REFERENCES

Constable, S., and L. J. Srnka, 2007, An introduction to marine controlled-source electromagnetic methods for hydrocarbon exploration: Geophysics, 72, no. 2, WA3–WA12.

de la Kethulle de Ryhove, S., and F. Maaø, 2008, On the removal of MT signals from SBL data: 70th Annual Conference and Exhibition, EAGE, Extended Abstracts, H047.

Jing, C., K. Green, and D. Willen, 2008, CSEM inversion: Impact of anisotropy, data coverage, and initial models: 78th Annual International Meeting, SEG, Expanded Abstracts, 604–608.

Mittet, R., L. Løseth, and S. Ellingsrud, 2004, Inversion of SBL data acquired in shallow waters: 66th Annual Conference and Exhibition, EAGE, Extended Abstracts, E020.

Morten, J. P., A. K. Bjørke, T. Støren, E. Coward, S. A. Karlsen, and F. Roth, 2009, Importance of azimuth data for 3D inversion of marine CSEM scanning data: 71st Annual Conference and Exhibition, EAGE, Extended Abstracts.

Støren, T., J. J. Zach, and F. Maaø, 2008, Gradient calculations for 3D inversion of CSEM data using a fast finite-difference time-domain modeling code: 70th Annual Conference and Exhibition, EAGE, Extended Abstracts, P194.

Tarantola, A., 2004, Inverse problem theory and model parameter estimation: Society for Industrial and Applied Mathematics.

Zach, J. J., F. Roth, and H. Yuan, 2008, Data preprocessing and starting model preparation for 3D inversion of marine CSEM surveys: 70th Annual Conference and Exhibition, EAGE, Extended Abstracts, G003.